Advantages of PM-machines Compared to Induction Machines in Terms of Efficiency and Sensorless Control in Traction Applications

Florian Demmelmayr, Markus Troyer, Manfred Schroedl
Institute of Energy Systems and Electrical Drives
Vienna University of Technology, Vienna, Austria
florian.demmelmayr@tuwien.ac.at, http://www.ieam.tuwien.ac.at/

***Abstract*—The energy consumption of a permanent magnet synchronous machine (PMSM) is compared with the model of an induction machine (IM). Both machines are wheel-hub traction drives and developed for electric tramways. An overview contrasts the ability of sensorless control for the two machine types at different machine speed. The *Indirect Flux detection by Online Reactance Measurement* (INFORM) method at standstill and low speed and a back-EMF model at high speed provide sensorless control of the PMSM over the whole speed range. The quality characteristic of the two approaches (depending on speed and load), the implemented control structure and the influence of the INFORM test sequences on produced torque are discussed.**

***Index Terms*—electric drive, energy consumption, sensorless control**

I. Introduction

Energy efficiency and sensorless control are two important aspects of electrical traction drives. High efficiency drives play a significant role in saving energy. Lower energy consumption increases environmental sustainability and decreases operating costs of electric drive systems. At the moment, most electric drives for electric trams work with induction machines (IMs) but nowadays also permanent magnet synchronous machines (PMSMs) become more popular. The two machine types provide different efficiency values at different operation points. Therefore significant comparisons of the energy consumption need specified operation behavior. This paper compares the energy consumption of a PMSM and an IM, designed for electric trams. A typical drive cycle classifies the points of the efficiency maps and enables significant comparison of the energy saving potential.

Sensorless control of electric machines enables rotor position estimation without the use of position encoders. The often used fault-prone encoders decrease the reliability of the whole drive and also increase the price. Sensorless control methods are used to improve reliability and robustness. The behavior of different sensorless control methods mostly depends on the machine speed. At high speed, well-established EMF methods handle the position detection but do not work at low speed or rather at standstill. At this operating range, the *Indirect Flux detection by Online Reactance Measurement* (INFORM) model is a practicable alternative to estimate the rotor angular position. This paper presents the implemented INFORM method, which works well up to high overload. Additionally the quality of the INFORM and EMF method are compared over load and machine speed. Also the influence of the used INFORM test signals on produced torque is shown.

II. Wheel hub drives for electrical tramway

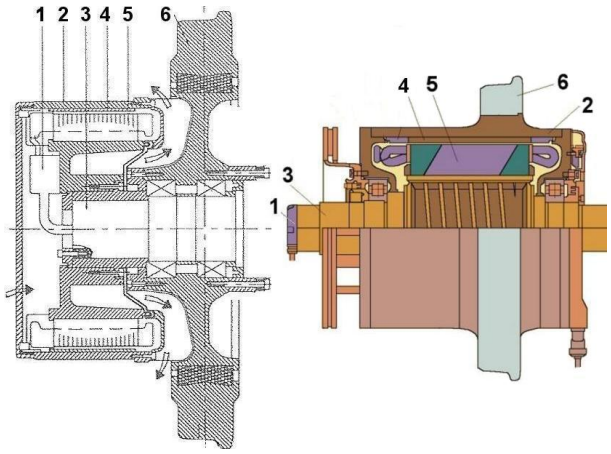

Fig. 1. Left: Layout of a synchronous drive for motorized wheels without gearbox for light rail systems [1]. Right: Sectional view of an induction machine in wheel hub configuration for a tramway, model 8 WXA3442 DaimlerChrysler Rail Systems (Austria) [2]. Terminal unit (1), housing (2), shaft (3), rotor (4), stator (5) and wheel (6)

Outer rotor machines for wheel hub drives are well known. Two examples are shown in figure 1, further details are presented in [1], [2] and [3].

With the support of our industrial partner Voith Turbo GmbH (St. Pölten, Austria) a novel wheel hub drive was developed (fig. 2), built (fig. 3) and tested. This PMSM works without position encoder and reaches a maximum torque of 4000 Nm.

III. Sensorless control

At high speed position sensorless or also called encoderless control of PMSMs and IMs is state-of-the-art (e.g. [4] - [8]). Beyond 10 - 20 % of nominal speed, most methods deal with induced voltages (back EMF) which can hardly be measured at low speed and disappear at standstill. The flux position is not observable at zero stator flux frequency in case of IM.

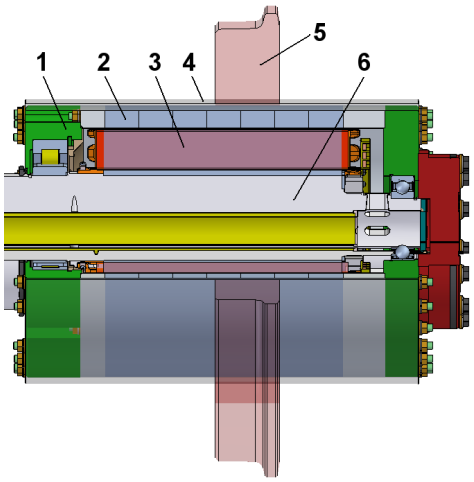

Fig. 2. Layout of the PMSM prototype: bearing shield (1), rotor with permanent magnets (2), stator (3), housing (4), wheel (5) and shaft (6)

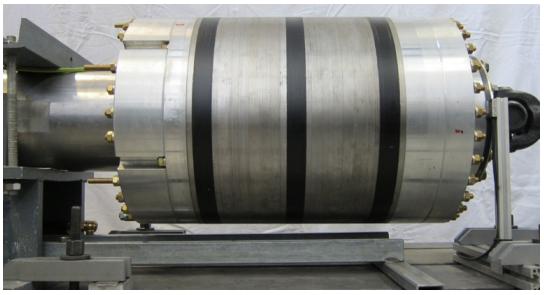

Fig. 3. Picture of the PMSM

Much research deal with back EMF signals but the outcomes are not commercially used until now (e.g. [7], [8]). Mechanical standstill can be controlled using extendend machine models but zero stator flux is critical. INFORM control ([9] and chapter III-A) for PMSMs also works at zero speed. The whole control of the presented drive uses two different models, an EMF based approach and the INFORM method at zero and low speed.

A. Basic idea of the INFORM method

INFORM uses inductance changes due to reluctance and/or saturation, depending on the angular rotor position of the PMSM. These varying magnetic properties are detected by active test signals which interrupt the normal pulse-width modulation (PWM) of the inverter. The interrupts occur only for a very short time period and only in certain intervals.
The inductance changes $\underline{l}_{\text{inc}}$ are determined by the current response $\Delta\,\underline{i}_{\text{s}}/\Delta\,\tau$ applied by the test voltage steps $\underline{u}_{\text{s}}$

$$\underline{l}_{\text{inc}} := \frac{\underline{u}_{\text{s}}}{\Delta\,\underline{i}_{\text{s}}/\Delta\,\tau}. \tag{1}$$

Saturation and reluctance effects have an electrical angular symmetry of 180° and therefore also the incremental inductance $\underline{l}_{\text{inc}}$ and its inverse

$$\underline{y}_{\text{INF}} := \frac{1}{\underline{l}_{\text{inc}}} \tag{2}$$

display this behavior. $\underline{y}_{\text{INF}}$ describes a circle in the Gaussian plane and is used to calculate the rotor position of the presented traction drive. It consists of an offset y_0 and the mentioned circle (radius Δy) which argument is a function of the stator voltage space phasor angle γ_{U} and the searched rotor position γ_{m}

$$\underline{y}_{\text{INF}} := y_0 + \Delta y \cdot e^{\jmath(2\,\gamma_{\text{m}} - 2\,\gamma_{\text{U}})}. \tag{3}$$

The current changes of the test signals are typically measured in all three phases (stator voltage space phasor angle γ_{u}, γ_{v} or γ_{w}). The voltage test signal consists of one voltage step in each phase (fig. 4) alternating positive and negative with a duration $t_{\text{sequence}} = 0.72\,\text{ms}$. The signals are applied with a frequency of 333 Hz.

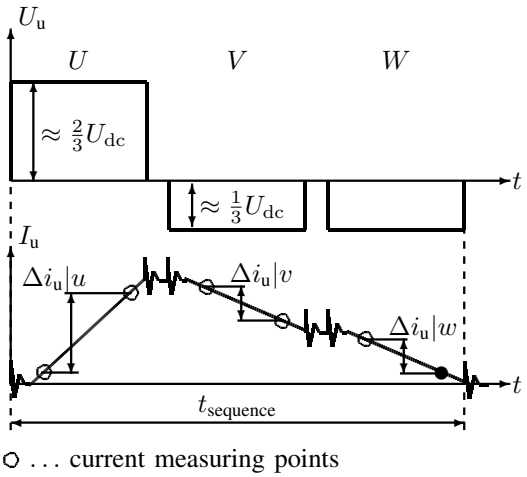

Fig. 4. Voltage test signals U_{u} and current responses I_{u} during the INFORM measurement in phase u with three cyclic voltage signals U, V and W [10]

The combination of the measurements in all three phases yields three complex current changes $\Delta\underline{i}|u$, $\Delta\underline{i}|v$ and $\Delta\underline{i}|w$ from figure 5. Each complex quantity has two different outcomes, one from the real and one from the imaginary part. Therefore six equations for the three unknown values y_0, Δy and $2\,\gamma_{\text{m}}$ are available. Both, real and imaginary part exploitation result in the components of equation (3).
The outcomes of the calculation, the so-called "Characteristic INFORM curve", are compared in section IV-D. Instead of estimated circles, the shapes of the curves are similar to triangles because of higher harmonics.

B. Structure of the sensorless INFORM/EMF control

The control structure of the whole speed range is shown in Fig. 6 and a similar approach is explained in [11].

1) Reference frame transformation: The actual direct ($i_{\text{d,meas}}$) and quadrature ($i_{\text{q,meas}}$) stator current components are calculated with Park's Transformation [12] from the measured phase currents (i_{u}, i_{v}, i_{w}) with the use of the estimated rotor angle $\hat{\gamma}$.

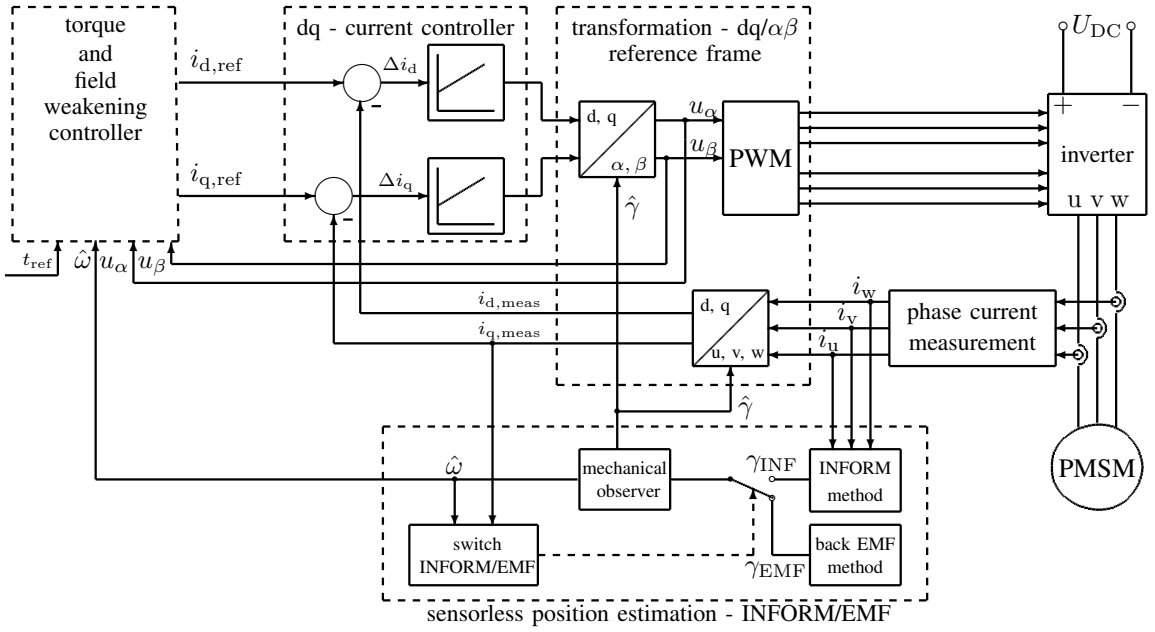

Fig. 6. Control structure for the drive [11]

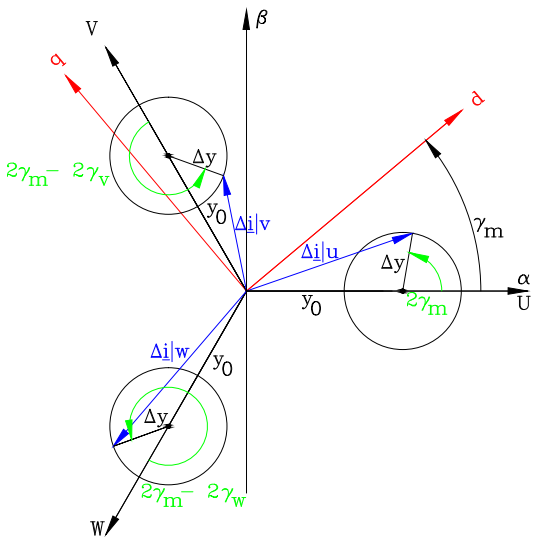

Fig. 5. Rotor position dependent current changes [13]

2) Switch between sensorless methods: The actual rotor speed ($\hat{\omega}$), which is calculated by a mechanical observer (fig. 7), and the quadrature stator current component ($i_{q,meas}$) decide which model is selected, the INFORM (γ_{INF}) for standstill and low speed or the EMF (γ_{EMF}) for high speed. The switch operates with a hysteresis to prohibit unwanted toggle between the two sensorless methods.

3) Mechanical observer: The mechanical observer improves the sensorless position information and determines the actual rotor speed ($\hat{\omega}$) [13]. The input of the observer ($\Delta\gamma$) is the output signal of the switch and therefore the difference between sensorless estimation (γ_{EMF} or $2\gamma_{INF}$) and the actual

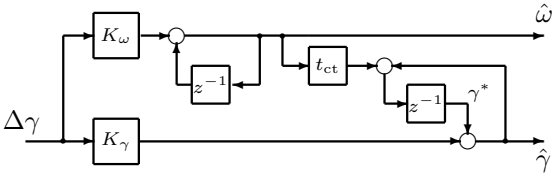

Fig. 7. Mechanical observer [13]

observed rotor position (γ^* or $2\gamma^*$),

$$\text{EMF method:} \quad \Delta\gamma = \gamma_{EMF} - \gamma^* \tag{4}$$

or

$$\text{INFORM method:} \quad \Delta\gamma = 2\gamma_{INF} - 2\gamma^*. \tag{5}$$

The constants K_ω and K_γ affect the outcome of the speed and the angle calculation. They quantify the values from sensorless estimation and the observer. The whole structure from figure 7 is implemented by using the microcontroller of the drive inverter. Each software task of the controller calculates a new position value. The actual rotor speed ($\hat{\omega}$) influences the angle estimation of the next task. The normalized dead time t_{ct} considers the time between two tasks of the used controller. Equations 6 and 7 describe the oberserver structure in the discrete z-domain.

$$\hat{\gamma} = K_\gamma \cdot \Delta\gamma + z^{-1} \cdot (\hat{\omega} \cdot t_{ct} + \hat{\gamma}) \tag{6}$$

$$\hat{\omega} = K_\omega \cdot \Delta\gamma + z^{-1} \cdot \hat{\omega} \tag{7}$$

4) Torque and field weakening controller: The torque and field weakening controller uses the estimated rotor speed, the reference torque from the tramway driving system and the components of the voltage space phasor u_α and u_β. The reference space phasor currents, inputs of the current

controller, in direct ($i_{\mathrm{d,ref}}$) and quadrature ($i_{\mathrm{q,ref}}$) axis are determined by the knowledge of the efficiency curve of the PMSM (fig. 8). The efficiency value and the corresponding current space phasor of each torque/speed point enable optimal effective operation of the traction drive including the reluctance torque. This controller also handles the field weakening strategy at high speed.

5) Current controller: The current controller consists of two separate parts which have a PI structure. The transformations between the rotor oriented dq and the stator oriented $\alpha\,\beta$ reference frame are based on the improved rotor position $\hat{\gamma}$ from the sensorless position estimation.

IV. Measurements and Results

The measurements of the PMSM prototype are realized on a test bed with a DC load machine. A digital torque transducer detected machine speed and torque. Electrical values are recorded by a precision power meter. The rotor positon of the sensorless methods are measured by oscilloscope.

A. Machine efficiency curves

The color fields of the machine efficiency curves (PMSM fig. 8 and IM fig. 9) represent different efficiency values in a torque over machine speed graphic.
The points of the PMSM map are recorded at steady state and consider the machine efficiency but not the inverter losses. The figure includes the reluctance torque to enlarge the output torque at given stator current magnitude. This necessitates a negative direct current component beside the main current component in quadrature axis. The blue crosses highlight the different discrete time points of the drive cycle explained in section IV-B.

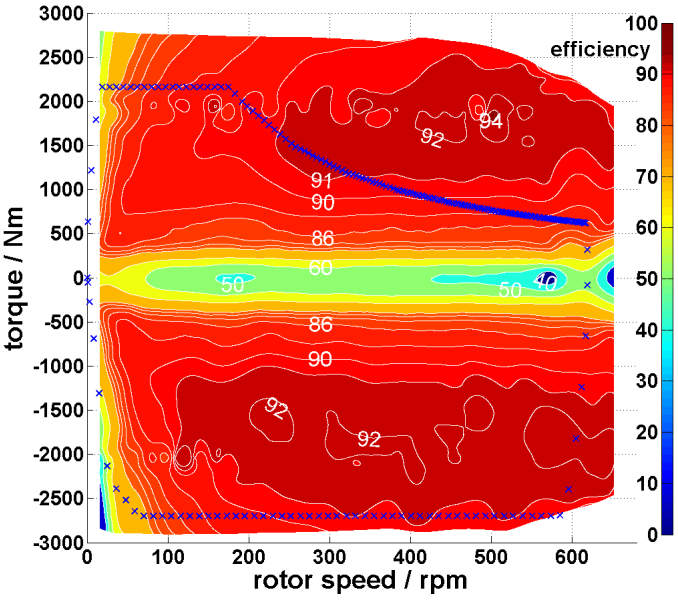

Fig. 8. Measured machine efficiency curve of the PMSM

The machine efficiency curve of the IM (fig. 9) is calculated from an induction machine model based on real data similar to [3]. The numerical simulation of this machine assumes inverter-fed operation. The iron losses are regarded parallel to an ordinary equivalent circuit diagram with known parameters in nominal operation point. The control (voltage-frequency) characteristic of the inverter considers a minimum startup voltage and field weakening at high speed. Again the blue crosses in figure 9 represent the discrete drive cycle points. The calculated machine efficiency map provides a good quantitative value for comparison of the energy consumption of the IM and the PMSM (section IV-B).

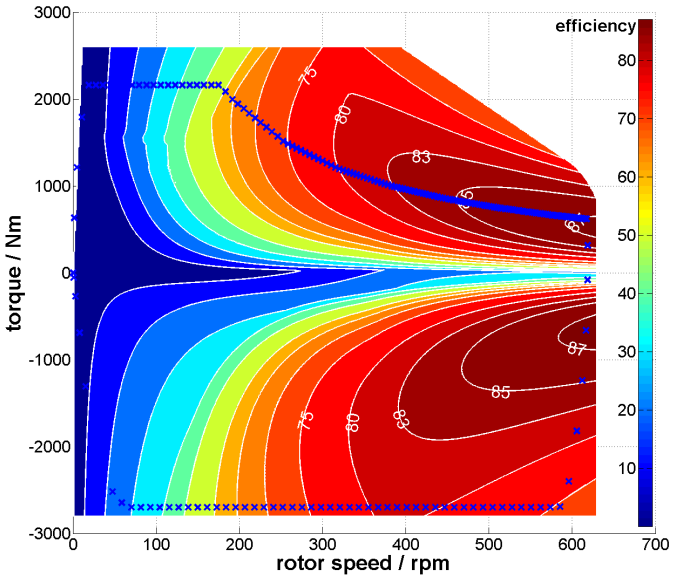

Fig. 9. Machine efficiency curve of the modeled IM

B. Drive cycle and energy consumption

The energy consumption of the developed PMSM and the calculated model of the IM are analysed over one drive cycle, shown in figure 10. The presented speed and torque versus

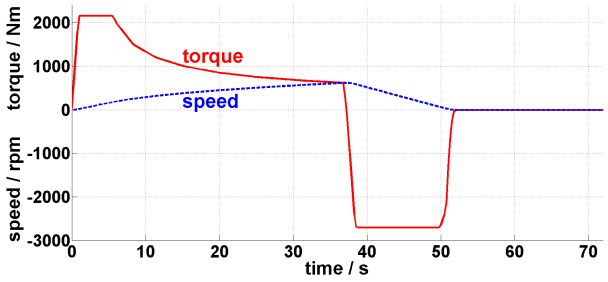

Fig. 10. Drive cycle of a typical electric tram

time graphs are typical for electric city trams and are specified by our industrial partner Voith Turbo GmbH. Initially the drive accelerates at constant torque of 2200 Nm for 5.5 seconds. After a reduction to 315 Nm the machine reaches the point of maximum speed at 620 rpm. Deceleration with 2700 Nm stops the drive after 11 seconds. The final period of standstill leads to a duration time of 72 seconds.

The curves of the specified drive cycle are divided into discrete time steps Δt = 0.25 seconds. These discrete points are inserted in the measured efficiency map of the PMSM (fig. 8) and the calculated graphic of the IM (fig. 9). The combination of torque T_i, rotor speed n_i, related efficiency η_i and the time duration Δt leads to input and output work of each point.
Motor operation ($T_\mathrm{i} > 0$, index m) contains 149 steps. The electrical input work is calculated by

$$W_{\mathrm{el,m}} = \sum_{i=1}^{149} \frac{2\pi \cdot T_\mathrm{i} \cdot n_\mathrm{i} \cdot \Delta t}{60 \cdot \eta_\mathrm{i}} \tag{8}$$

Breaking operation ($T_\mathrm{i} \leq 0$, index b) contains 140 steps. Equation (9) shows the electrical output work.

$$W_{\mathrm{el,b}} = \sum_{i=1}^{140} \frac{2\pi \cdot T_\mathrm{i} \cdot n_\mathrm{i} \cdot \eta_\mathrm{i} \cdot \Delta t}{60} \tag{9}$$

The electrical energy consumption, here also the lost energy W_lost, over the whole drive cycle is calculated by

$$W_\mathrm{lost} = W_{\mathrm{el,m}} + W_{\mathrm{el,b}}. \tag{10}$$

	PMSM	IM
$W_{\mathrm{el,m}}$	1544 kWs	1922 kWs
$W_{\mathrm{el,b}}$	-1024 kWs	-863 kWs
W_lost	520 kWs	1059 kWs

TABLE I
ENERGY CONSUMPTION

Some points of highest speed and negative torque of the PMSM are outside the measured efficiency map. Field weakening reduces the maximum reachable torque because of the limited inverter supply voltage on the test stand. The efficiency of this missing points is assumed by 80 % for calculation of the energy consumption.
The DC load machine cannot operate at very low speed. The missing points below 15 rpm are assumed by efficiency values of 10 %.
Compared to the lost energy of the IM (100 %) the energy consumption of the PMSM is only 49 %. Therefore the PMSM offers a energy saving potential of more than a half.
A high direct stator inductance l_d enables field weakening at very low additional copper losses by a field weakening current component in negative direct axis. This behavior leads to high efficiency values of a PMSM up to high field weakening range.

C. Quality of the sensorless control methods of the PMSM

The difference between the actual rotor position, measured with a position encoder, and the angle from the sensorless calculation is recorded at different speed and load. The standard deviations of these differences act as quality characteristic of the INFORM and EMF method and they are used to switch between the two different sensorless operation modes. Figures 11 and 12 compare the raw signals (γ_INF and γ_EMF), which are imputs of the mechanical observer. The INFORM method (fig. 11) compensates the induced back-EMF by special test seqences and has its highest reliability (standard deviation between 6° and 8°) at standstill and low speed. The vanishing back-EMF is a benefit for INFORM but a great disadvantage for EMF (fig. 12). The performance of the EMF method significantly decreases at higher current.

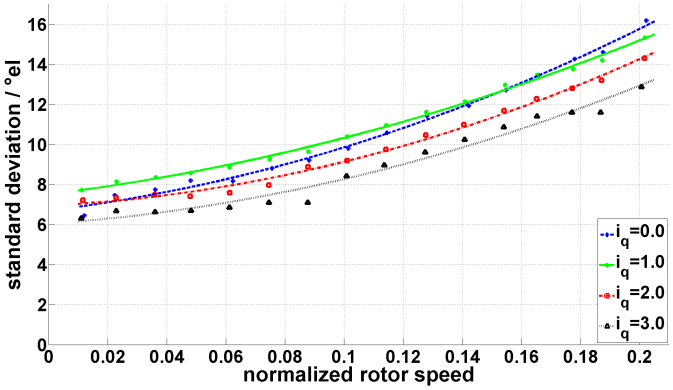

Fig. 11. Standard deviation of the difference between angle from INFORM and angle from encoder

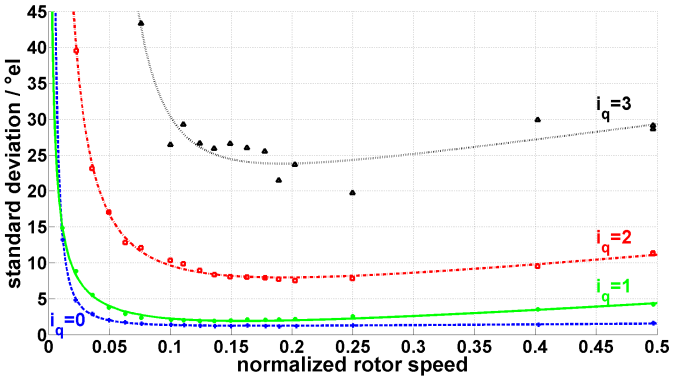

Fig. 12. Standard deviation of the difference between angle from EMF and angle from encoder

The mechanical observer improves the quality of the encoderless control (fig. 13 and 14). On the other hand below 5 % of rated speed the mechanical observer reduces the performance of the INFORM method. A speed dependent feedback coefficient is recommended to correct this behavior.

D. Curves from the INFORM measurement

The INFORM curves at different machine speed are depicted from fig. 15 to 18. They present equation 3 in a complex plane. At low speed the curves are similar triangles with a 180° electrical symmetry. The shape of the INFORM curves are sensitive to north and south magnetic pole especially at high speed and high load. Experience has shown that the sensorless control becomes useless over 10° standard deviation. From fig. 18 it can be seen, that INFORM should not be used at high speed and i_q=3.

Figure 19 shows the relation between the approached circle offset (y_0) and the circle radius (Δy) from equation 3 at no

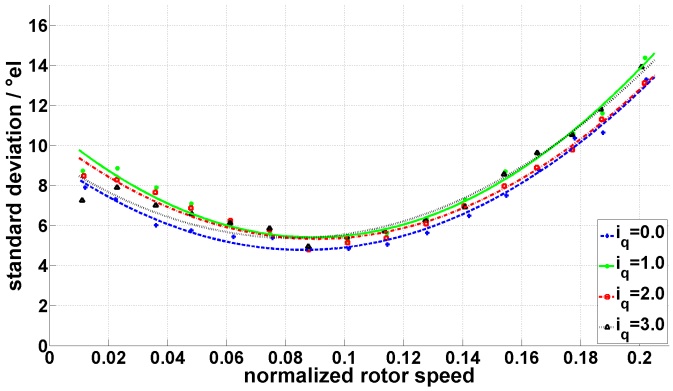

Fig. 13. Standard deviation of the difference between angle from INFORM and angle from encoder corrected by the mechanical observer

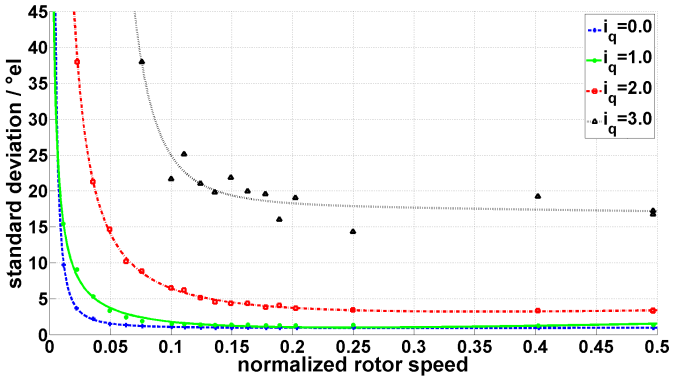

Fig. 14. Standard deviation of the difference between angle from EMF and angle from encoder corrected by the mechanical observer

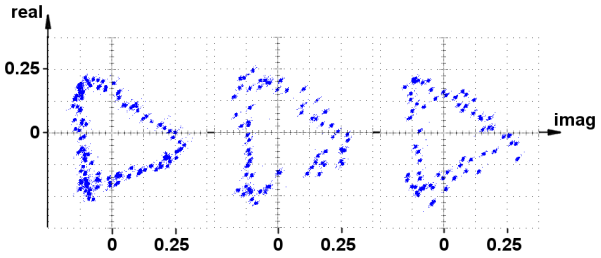

Fig. 15. Characteristic INFORM curves at no load, ω = 0.01, 0.1 and 0.2

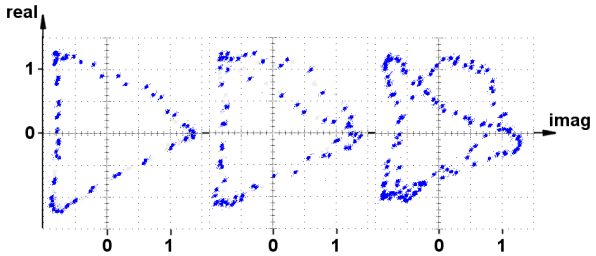

Fig. 16. Characteristic INFORM curves at $i_q = 1$, ω = 0.01, 0.1 and 0.2

load and nominal quadrature stator current. The ratio $\frac{\Delta y}{y_0}$ rises from 0.16 ($i_\mathrm{q} = 0$) to 0.35 ($i_\mathrm{q} = 1$). This behavior results in a higher signal to noise ratio and therfore increases the quality

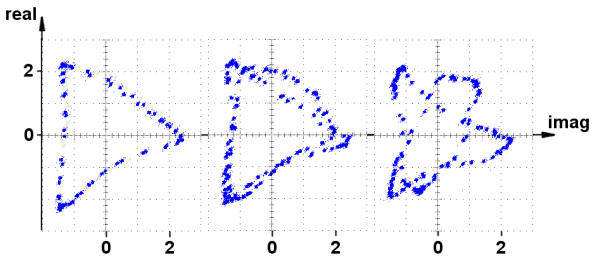

Fig. 17. Characteristic INFORM curves at $i_q = 2$, ω = 0.01, 0.1 and 0.2

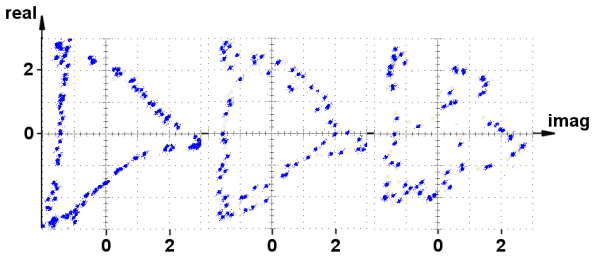

Fig. 18. Characteristic INFORM curves at $i_q = 3$, ω = 0.01, 0.1 and 0.2

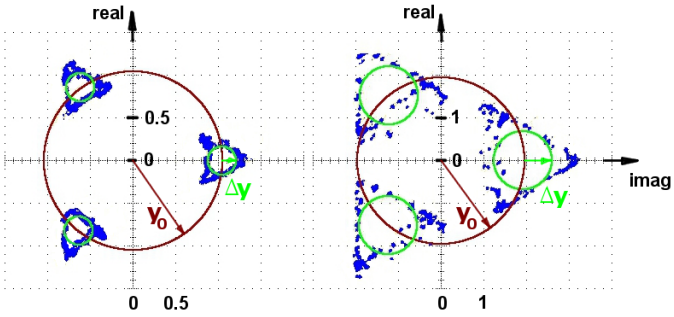

Fig. 19. Current changes $\Delta\underline{i}|u$, $\Delta\underline{i}|v$ and $\Delta\underline{i}|w$ from INFORM method at no load (left) and $i_q = 1$ (ω = 0.01)

of the INFORM method with rising load.

E. Influence of the active test pulses on average torque

The INFORM method at low speed interrupts the ordinary pulse width modulation (PWM) sequence of the inverter during short time intervals. Also the torque production of the drive is interrupted by the active test pulses. Figure 20 compares the output torque including the influence of the encoderless INFORM position measurement with an ordinary control with position encoder. The two curves are printed over stator current RMS values at a rated machine speed of 0.01. The sensorless method has only a small influence.
The figure also depicts the ”Characteristic INFORM curves” (eq. (3)) at no-load, 1/3, 2/3 and maximum current. The signals are printed without an additional magnification factor and represent the size of the curves over different load.

V. Conclusion

The presented PMSM prototype offers an energy saving potential of 51 % compared to an IM drive over a characteristic drive cycle. At zero stator flux frequency the rotor position

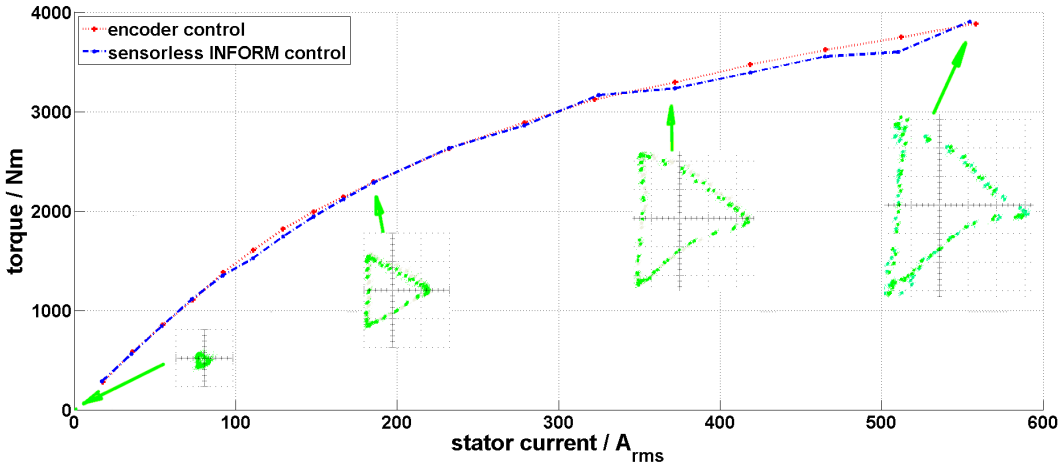

Fig. 20. Torque over stator current magnitude with "Characteristic INFORM curves" at selected operation points

estimation of IMs is very difficult. The discussed sensorless control structure of the PMSM with INFORM and EMF combines the advantages of each method over the whole speed range. The quality influence of the load on the sensorless position calculation can be improved by a mechanical observer.

REFERENCES

[1] G. Braga, A. Farini, R. Manigrasso, *Synchronous drive for motorized wheels without gearbox for light rail systems and electric cars.*, Proc. EPE Conference Firenze, Italy, 4, 78-81, 1991.

[2] H. Neudorfer, *Radnabenmotoren in Asynchron-Außenläufertechnik für den Antrieb von Niederflur-Stadtbahnfahrzeugen*, ZEV + DET Glas.Ann. 125 6/7 Juni/Juli. 2001

[3] W. Hackmann, *Systemvergleich unterschiedlicher Radnabenantriebe für den Schienennahverkehr: Asynchronmaschine, permanenterregte Synchronmschine, Transversalflussmaschine*, Doctoral thesis, Technische Universität Darmstadt, 2003

[4] R. Wu, G.R. Slemon, *A permanent magnet motor drive without a shaft sensor*, IEEE Trans. Industrial Appl., vol.27, pp. 1005-1011,1991.

[5] D. Paulus, J.-F. Stumper, P. Landsmann, R. Kennel, *Robust Encoderless Speed Control of a Synchronous Machine by direct Evaluation of the Back-EMF Angle without Observer*, Sensorless Control of Electrical Drives (SLED), Padova, Italy, 2010

[6] M. Corley, R. Lorenz, *A Rotor position and velocity estimation for permanent magnet synchronous machines at standstill and high speed* IEEE IAS Conf. Proc. 1996, S.36-41.

[7] T.M. Wolbank, R. Woehrnschimmel, *Evaluation of lamination materials in zero-speed sensorless controlled induction machine drives* Electrical and Electronic Technology, TENCON, Singapore, 2001.

[8] Q. Gao, G.M. Asher, M. Sumner, and P. Makys, *Position estimation of AC machines over a wide frequency range based on space vector PWM excitation*, IEEE Trans. Ind. Appl., vol. 43, no. 4, pp. 10011011, Jul./Aug. 2007.

[9] M. Schroedl, *Sensorless control of AC machines at low speed and standstill based on the "INFORM" method*, IEEE IAS Conference, San Diego, Proc. 1: 270-277, 1996.

[10] A. Eilenberger, *Permanent Magnet Synchronous Machines With Tooth Coils for Sensorless Control Including Overload Range*, Doctoral thesis, Vienna University of Technology, 2011

[11] M. Schroedl, W. Staffler, *Sensorless Control of a Double-Stator Disc Rotor PM Synchronous Motor Using a Combined INFORM®/EMF Model*, Power Conversion Intelligent Motion (PCIM), Germany, Nürnberg, May 2009

[12] R.H. Park, *Two-Reaction Theory of Synchronous Machines Generalized Method of Analysis - Part I*, Transactions of the American Institute of Electrical Engineers (AIEE), New York, N.Y., Vol. 48. pp.716-727, July 1929

[13] F. Demmelmayr, M. Susic, M. Schroedl *Sensorless Control at High Starting Torque of a 4000 Nm Traction Drive With Permanent Magnet Synchronous Machine*, European Power Electronics and Drives (EPE), Birmingham, UK., 2011